POLITECNICO
MILANO 1863

SCUOLA DI INGEGNERIA INDUSTRIALE
E DELL'INFORMAZIONE

Homework report

Homework 2

Scientific computing tools for advanced mathematical modelling

Authors: Davide Carrara - Luca Sosta - Daniela Zanotti

Academic year: 2021-2022

---

1. Mathematical formulation of the problem

1.1. Description of the problem

A stroke is a pathological condition in which the blood flow to the brain is stopped. The most common cause is the formation of a blood clot (thrombus), most atrial thrombi form in the left atrial appendage (LAA), with greater or lesser incidence depending on the patient morphology. Many studies have investigated this variability using imaging techniques.

Four principal forms (reported in Figure 1, taken from this article [1]) have been identified:

- cactus
- chicken wing
- windsock
- cauliflower

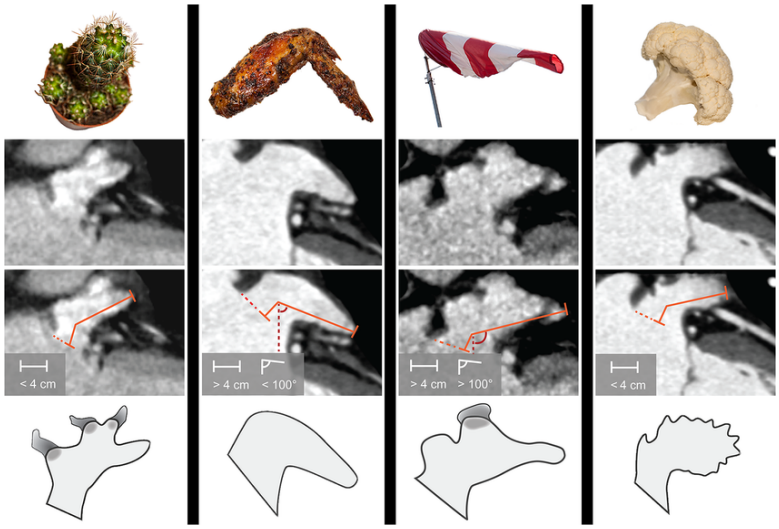

Figure 1: Principal shapes

1.2. RBF Models

We chose to define our shape model starting from the template mesh provided for the problem, and generated the shapes representing the four main forms by deformation of the template using a limited amount of control points. The displacement of the various points of the mesh can then be derived using the following shape model equations.

$$\tau(\bar{x}, \mu) = \rho(\bar{x}) + \sum_{i=1}^{i=k} \bar{\omega}(\mu) \cdot \phi(\|\bar{x} - \bar{x}_i\|)$$

Where:

- $\tau(\cdot, \mu)$ represents the transformation from the original shape to the new one;
- $\phi(\cdot)$ is the radial basis function, and its particular choice will be discussed in the following section;
- $\rho(\bar{x})$ corresponds to a part of the movement which does not depend on the control points (usually an affine transformation, representing rotation or translation). However, we chose to use the identity function, mapping $\bar{x}$ in itself.

The weights can be collected into a matrix $\mathrm{W} \in \mathbb{R}^{\mathrm{k\ x\ d}}$, where k is the number of control points and d the dimensionality of the points (two in this specific case).
In this case, the matrix W can be computed by solving the following linear system:

$$\begin{bmatrix} \phi(\|\bar{x}_1 - \bar{x}_1\|) & \dots & \phi(\|\bar{x}_1 - \bar{x}_k\|) \\ \vdots & \ddots & \\ & & \phi(\|\bar{x}_k - \bar{x}_k\|) \end{bmatrix} \quad \mathbf{W} \quad = \quad \begin{bmatrix} \delta_{1,x} & \delta_{1,y} \\ \vdots & \vdots \\ \delta_{k,x} & \delta_{k,y} \end{bmatrix}$$

where δ represents the displacement assigned to each control point.

The key aspect of this kind of shape models is the use of Radial Basis Function, which express as a weighted sum the effect that any control point has on each point of the mesh.

1.3. Pros and Cons

This approach presents some evident pros and cons.

The method is in itself extremely flexible, as any kind of shape can be reached starting from the template. Unfortunately this is only theoretically useful: in order to obtain complicated shapes an increasing number of control points is needed. However:

- since we are not re-meshing each time, the probability of obtaining invalid meshes increases with the number of control points;
- the generalization property of the model would diminish, as we would tend to overfit specific behaviours of a single patient rather than the generic shape.

The choice of generating all the meshes from a single template without re-meshing provides however some significant strength to our analysis:

- first of all, we can establish a 1-to-1 correspondence between each point of the mesh among the different shapes. This means that it is possible not only to produce a generic analysis, but also to compare specific and local behaviours of our quantities of interest;
- it is also possible to move from one of the four forms to the other in a smooth way, by interpolation of the control points displacements. This is particularly useful in a real case scenario, where a patient could be more precisely represented by an intermediate shape;
- lastly, it is possible, from an applicative point of view, to move between different shapes using significant control points such as the extreme point of the Left Atrial Appendix.

In general compared to a small loss in precision, we have a bigger gain from the point of view of **interpretability**.

2. Methods

2.1. Radial Basis Function

We considered different kind of radial basis functions, ending up with the most common gaussians one. Given the same control points these functions combine regularity and flexibility in the best way, providing a good representation of each template. The considered functions are reported below:

$$\text{Gaussian}: \phi(\|x-y\|) = \exp\left(-\frac{\|x-y\|_2^2}{\sigma^2}\right)$$

$$\text{Laplacian}: \phi(\|x-y\|) = \exp\left(-\frac{\|x-y\|_1}{\sigma}\right)$$

$$\text{Elastic}: \phi(\|x-y\|) = \exp\left(-\frac{\|x-y\|_1}{\sigma} - \frac{\|x-y\|_2^2}{\sigma^2}\right)$$

$$\text{Inverse}: \phi(\|x-y\|) = \left(\frac{1}{\sqrt{\|x-y\|_2^2 + \sigma^2}}\right)$$

It is worth noticing that these functions depend only on the distance between the two points providing thus a simplified model. We can see the different representations of the Chicken Wing form using the various RBF.

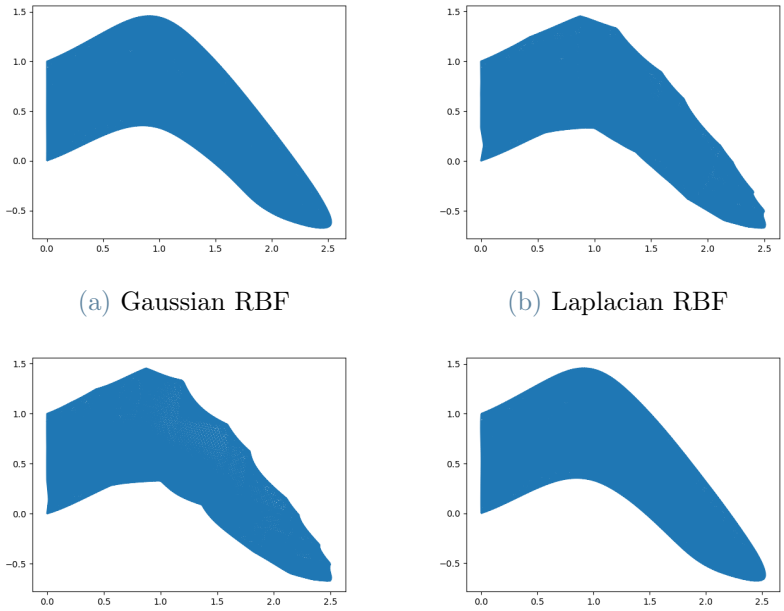

(a) Gaussian RBF (b) Laplacian RBF

(c) Elastic RBF (d) Inverse RBF

Figure 2: Shape model using the same control points but with different Radial Basis Functions

As we can see, Gaussian and Inverse RBF provide the best representation. However, the Gaussian one is more consistent with respect to small variations and is thus chosen.

2.2. Control Points

In order to provide a good representation of the different shapes without overfitting specifics behaviour, we chose to use the same 20 control points. Imposing the displacement for this points is sufficient to recreate the required shape. They are all positioned on the border of the template, and four of them are necessary to avoid deformations of the inlet.

The coordinates of the starting positions of the control points are reported here:

Table 1: Starting Coordinates of the Control Points

i	1	2	3	4	5	6	7	8	9	10
x	0	0	0	0	1	2.10	2	0.75	2.20	0.38
y	0	0.33	0.67	1	1.05	-0.15	-0.35	0.15	-0.35	0.13
i	11	12	13	14	15	16	17	18	19	20
x	1.15	1.70	1.72	1.32	0.29	0.14	0.68	1.80	1.47	1.98
y	0.02	-0.23	0.35	0.79	1.05	1.02	1.13	0.24	0.63	0.02

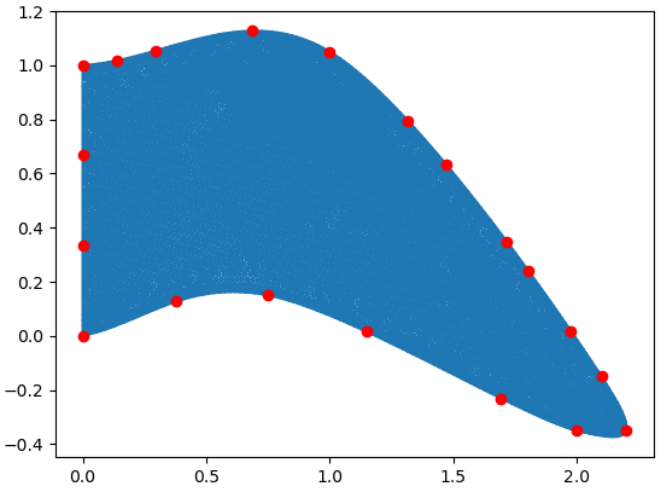

Figure 3: Control Points for the shape model

It is worth noticing that, in order to make our analysis more robust, we did not use just one single version of each shape, but we created 10 of them, introducing random deformations of the control points.

In particular we introduced these random deformations on the control points:

$$\text{Horizontal Noise} \sim N(0, 0.02^2)$$
$$\text{Vertical Noise} \sim N(0, 0.02^2)$$
$$\text{Horizontal Stretching} \sim N(1.1, 0.02^2)$$
$$\text{Rotation Angle} \sim U(-\frac{\pi}{8}, \frac{\pi}{8})$$

2.3. Numerical Solver Implementation

The physical problem is modelled as the well known cavity problem, so we have a straight section of the border where a parallel force is imposed and all the other forcing term are zero.
For the numerical simulation of the flow we used a Newton iterative method for the stationary Navier-Stokes equation. The solution is defined by the following iterative algorithm : given (u_{k-1}, p_{k-1}), the next iteration (u_k, p_k) is given by the solution of the linear problem:

$$\begin{cases} (\boldsymbol{u}_{k-1} \cdot \nabla)\boldsymbol{u}_k + (\boldsymbol{u}_k \cdot \nabla)\boldsymbol{u}_{k-1} - \frac{1}{Re}\Delta \boldsymbol{u}_k + \nabla \boldsymbol{p}_k = (\boldsymbol{u}_k \cdot \nabla)\boldsymbol{u}_k & \text{in } \Omega \\ \nabla \cdot \boldsymbol{u} = 0 & \text{in } \Omega \\ \boldsymbol{u} = -0.3\boldsymbol{j} & \text{on } \Gamma_{in} \\ \boldsymbol{u} = \boldsymbol{0} & \text{on } \Gamma_{wall} \end{cases}$$

where Ω is the whole LAA, Γ_{in} is the left border where there is the connection with the heart and Γ_{wall} is the reminder of the border.

The problem is then written in its weak form and solved with finite element through FreeFem++, starting the iterations with $(\boldsymbol{u}_0, \boldsymbol{p}_0) = (\boldsymbol{0}, \boldsymbol{0})$. Because the problem is also a fully Dirichlet problem the solution is well defined up to a constant for the pressure (it appears only through its gradient), so to guarantee the uniqueness of the solution we fix $\boldsymbol{p}_k = \boldsymbol{0}$ on the inlet border.

3. Numerical results

The goal of this homework is to define one or more indicators, that might help to predict the risk of ischemic stroke formation, comparing the different configurations. In order to make the comparison possible, the areas of the shapes must be of the same magnitude. The configurations created with the shape models have similar areas, except for the Chicken Wing, so we scaled the latter one multiplying all the control points by a shaping coefficient = 0.84. In this way we obtained comparable areas, as reported in the table.

Shape	Initial Areas	Final Areas
Chicken Wing	2.6763	1.8863
Windsock	2.0286	2.0286
Cactus	1.8321	1.8321
Cauliflower	1.7978	1.7978

Table 2: Areas of the shapes

At that point we defined a lot of indicators, such as:

- mean velocity
- max velocity
- absolute value of the curl
- percentage of area with negligible velocity ($<$ 1e-6 m/s)
- some quantiles of the velocity

The indicators have been computed as medians of the values obtained with 10 different versions of each shape. Analyzing their correlation, as expected, we found out that some of them are highly correlated, so we decided to keep only the absolute value of the curl and the percentage of area with negligible velocity. However, they cannot be combined together simply summing them, because they do not refer to the same quantity. Therefore we first have normalized them with respect to their mean and their variance, making the two comparable, and then we added them. The indicator obtained has larger values for morphology more inclined of forming a thrombus.

LAA Shape	Original Quantity | curl |	Original Quantity 0-velocity	Normalized Quantity | curl |	Normalized Quantity 0-velocity	Final Indicator
Chicken Wing	0.2283	0.1489	-0.1996	-0.9738	-1.1733
Windsock	0.1982	0.4394	-1.2414	1.1372	-0.1042
Cactus	0.2676	0.1876	1.1570	-0.6921	0.4648
Cauliflower	0.2424	0.3557	0.2840	0.5287	0.8127

Table 3: Indicators of stoke formation in different shapes

4. Conclusions

As we see from the table 3 above, Chicken Wing is considered the least dangerous left atrial appendix conformation. Its percentage of area with negligible velocity is by far the smallest among the four shapes, probably leading to a sufficient flow of blood in the cavity. This flow is, however, not particularly whirling (the mean value of the absolute curl its the second lowest among the shapes). As a consequence, this shapes avoid the formation of small vortices that could lead to coagulation an thrombuses.
The opposite argumentation holds for Cauliflower, the most dangerous shape. The indicators never assume the worst possible value for this shape, but the combination of bad performances is decisive in defining it as the worst conformation.

References

[1] Korhonen M, Muuronen A, Arponen O, Mustonen P, Hedman M, Jäkälä P, and et al. Left atrial appendage morphology in patients with suspected cardiogenic stroke without known atrial fibrillation.

Shapes

A. Chicken Wing

Table 4: Coordinates of Control Points for Chicken Wing

i	1	2	3	4	5	6	7	8	9	10
x	0	0	0	0	1.20	2.50	2.15	1	2.50	0.56
y	0	0.33	0.67	1	1.33	-0.50	-0.60	0.33	-0.67	0.28
i	11	12	13	14	15	16	17	18	19	20
x	1.36	1.82	2.11	1.59	0.43	0.21	0.87	2.22	1.79	2.40
y	0.09	-0.38	0.15	0.89	1.24	1.11	1.45	-0.01	0.62	-0.31

(a) Base Shape Model for Chicken Wing (b) Multiple Variations of Chicken Wing

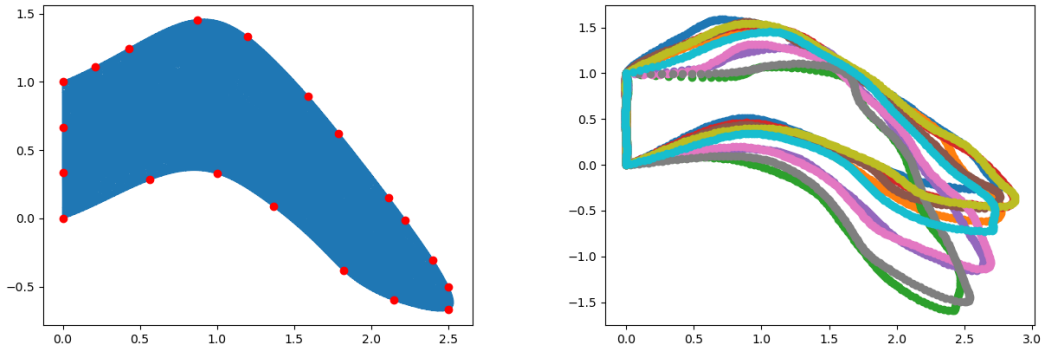

Figure 4: Shape model for the Chicken Wing

B. Windsock

Table 5: Coordinates of Control Points for Windsock

i	1	2	3	4	5	6	7	8	9	10
x	0	0	0	0	1.10	2.80	2.40	0.90	3	0.30
y	0	0.33	0.67	1	0.90	0.10	-0.03	0.20	-0.10	0.25
i	11	12	13	14	15	16	17	18	19	20
x	1.55	1.95	1.98	1.60	0.36	0.20	0.87	2.11	1.80	2.47
y	0.12	0.05	0.32	1.05	1	0.93	1.05	0.27	0.80	0.20

(a) Base Shape Model for Windsock

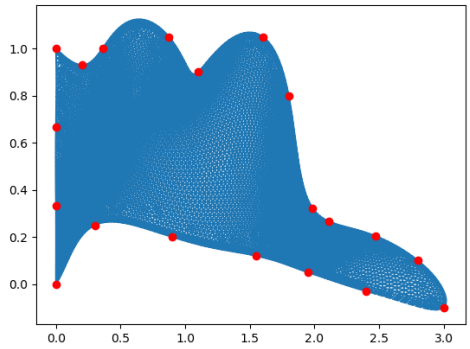

(b) Multiple Variations of Windsock

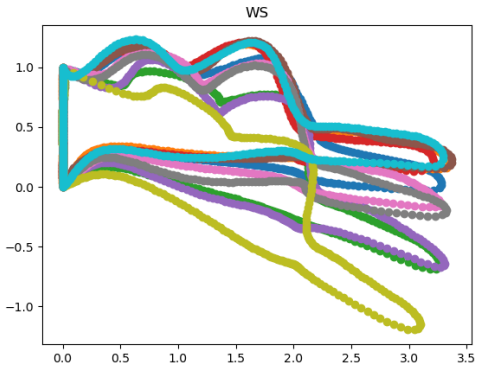

Figure 5: Shape model for the Windsock

C. Cactus

Table 6: Coordinates of Control Points for Cactus

i	1	2	3	4	5	6	7	8	9	10
x	0	0	0	0	1.10	1.75	1.72	0.80	1.90	0.40
y	0	0.33	0.67	1	0.85	-0.05	-0.30	0.15	-0.25	0.18
i	11	12	13	14	15	16	17	18	19	20
x	1.15	1.45	1.70	1.48	0.47	0.20	0.95	1.75	1.65	1.62
y	0.04	-0.20	0.47	0.82	1.10	1	1.20	0.35	0.68	0.15

(a) Base Shape Model for Cactus

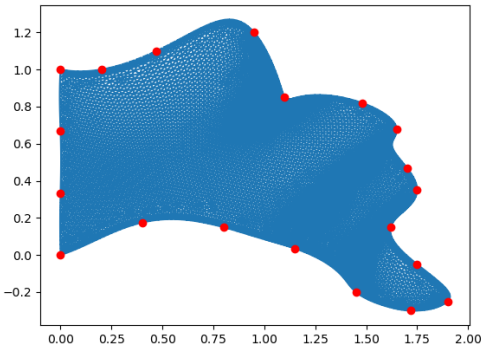

(b) Multiple Variations of Cactus

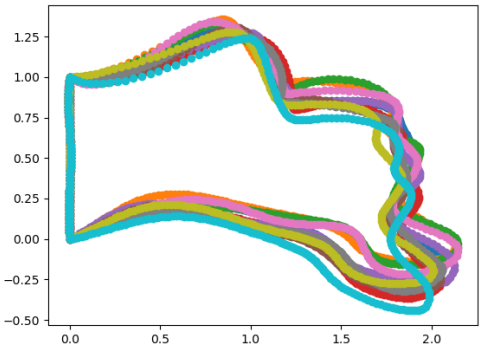

Figure 6: Shape model for the Cactus

D. Cauliflower

Table 7: Coordinates of Control Points for Cauliflower

i	1	2	3	4	5	6	7	8	9	10
x	0	0	0	0	1.20	1.80	1.58	0.60	1.80	0.25
y	0	0.33	0.67	1	1.15	0.10	-0.15	0.45	-0.20	0.25
i	11	12	13	14	15	16	17	18	19	20
x	0.95	1.25	1.65	1.40	0.55	0.30	0.85	1.80	1.65	1.85
y	0.08	-0.20	0.53	0.90	1.20	1.10	1.10	0.42	0.80	0.26

(a) Base Shape Model for Cauliflower (b) Multiple Variations of Cauliflower

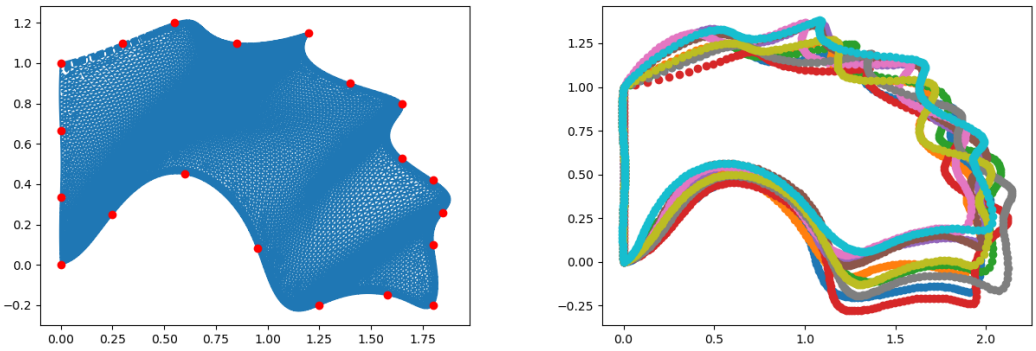

Figure 7: Shape model for the Cauliflower